Since January 2020 Elsevier has created a COVID-19 resource centre with free information in English and Mandarin on the novel coronavirus COVID-19. The COVID-19 resource centre is hosted on Elsevier Connect, the company's public news and information website.

Journal of Molecular Graphics and Modelling 101 (2020) 107762

Contents lists available at ScienceDirect

Journal of Molecular Graphics and Modelling

journal homepage: www.elsevier.com/locate/JMGM

Topical Perspectives

Prediction of potential inhibitors of the dimeric SARS-CoV2 main proteinase through the MM/GBSA approach

Martiniano Bello

Laboratorio de Modelado Molecular, Bioinformática y Diseño de Fármacos de La Escuela Superior de Medicina, Instituto Politécnico Nacional, México. Plan de San Luis Y Diaz Mirón S/N, Col. Casco de Santo Tomas, México City, CP, 11340, Mexico

A R T I C L E I N F O

Article history:
Received 4 April 2020
Received in revised form
15 September 2020
Accepted 21 September 2020
Available online 24 September 2020

Keywords:
SARS-CoV2
Proteinase
SARS-CoV
Docking
MD simulations

A B S T R A C T

Since the emergence of SARS-CoV2, to date, no effective antiviral drug has been approved to treat the disease, and no vaccine against SARS-CoV2 is available. Under this scenario, the combination of two HIV-1 protease inhibitors, lopinavir and ritonavir, has attracted attention since they have been previously employed against the SARS-CoV main proteinase (M^{pro}) and exhibited some signs of effectiveness. Recently, the 3D structure of SARS-CoV2 M^{pro} was constructed based on the monomeric SARS-CoV M^{pro} and employed to identify potential approved small inhibitors against SARS-CoV2 M^{pro}, allowing the selection of 15 drugs among 1903 approved drugs to be employed. In this study, we performed docking of these 15 approved drugs against the recently solved X-ray crystallography structure of SARS-CoV2 M^{pro} in the monomeric and dimeric states; the latter is the functional state that was determined in a biological context, and these were submitted to molecular dynamics (MD) simulations coupled with the molecular mechanics generalized Born surface area (MM/GBSA) approach to obtain insight into the inhibitory activity of these compounds. Similar studies were performed with lopinavir and ritonavir coupled to monomeric and dimeric SARS-CoV M^{pro} and SARS-CoV2 M^{pro} to compare the inhibitory differences. Our study provides the structural and energetic basis of the inhibitory properties of lopinavir and ritonavir on SARS-CoV M^{pro} and SARS-CoV2 M^{pro}, allowing us to identify two FDA-approved drugs that can be used against SARS-CoV2 M^{pro}. This study also demonstrated that drug discovery requires the dimeric state to obtain good results.

1. Introduction

In December 2019, another outbreak of acute respiratory disease caused by a novel coronavirus (CoV) was reported in Wuhan, China [1,2]. Analysis of the complete genome of severe acute respiratory syndrome coronavirus 2 (SARS-CoV2) demonstrated that it belongs to betacoronavirus, but it is different from severe acute respiratory syndrome coronavirus (SARS-CoV) and Middle East Respiratory coronavirus (MERS-CoV), which caused previous epidemics [1]. This new disease was named coronavirus disease 2019 (COVID-19), previously known as novel coronavirus [2019-nCoV], by the World Health Organization. COVID-19 was first reported in China, and it has now spread quickly to distant nations, including France and the USA. The number of cases within and outside China are increasing abruptly, and no drug has proved to be effective. Therefore, it is crucial to discover and develop drugs to treat the disease. An alternative treatment for COVID-19 is the combination of two HIV-1 protease inhibitors, lopinavir and ritonavir, which was an effective therapy previously used against SARS-CoV [3]. Previous theoretical studies demonstrated that lopinavir and ritonavir form stable complexes with the SARS-CoV main proteinase (SARS-CoV M^{pro}), with similar affinity [4]. Similar to SARS-CoV M^{pro}, the main proteinase of SARS-CoV2 (SARS-CoV2 M^{pro}) exhibits a crucial role in the proteolytic activity of replicase polyproteins, which are indispensable for viral replication. In addition, an alignment of SARS-CoV M^{pro} and SARS-CoV2 M^{pro} shows that they share a high percentage of sequence identity ($\geq$95%). Several theoretical studies have been performed to identify inhibitors against SARS-CoV M^{pro}. Xu et al. constructed a three-dimensional homology model of SARS-CoV2 M^{pro} based on SARS-CoV M^{pro} and screened it against 1903 drug inhibitors via protein modeling and virtual screening, highlighting nelfinavir as a potential inhibitor against SARS-CoV2 M^{pro} [5]. Using X-ray crystallography, the structure of SARS-CoV2 M^{pro} has recently been solved in complex with the inhibitor N3 (PDB ID: 6LU7), revealing that its structural topology is similar to

E-mail addresses: bellomartini@gmail.com, mbellor@ipn.mx.

https://doi.org/10.1016/j.jmgm.2020.107762
1093-3263/

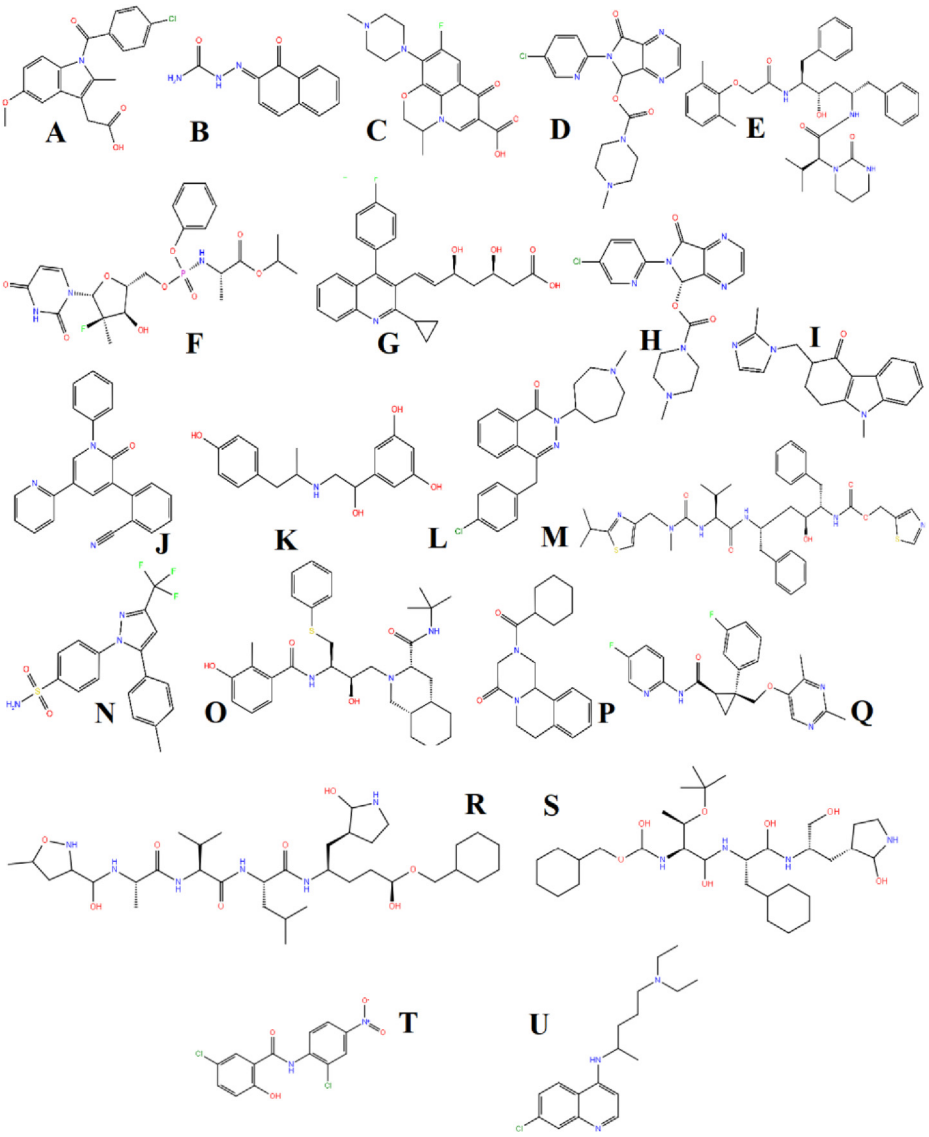

Scheme 1. 2D structure of the compounds used in this research. A) indomethacin, B) naftazone, C) ofloxacin, D) zopiclone, E) lopinavir, F) sofosbuvir, G) pitavastatin, H) eszopiclone, I) ondansetron, J) perampanel, K) fenoterol, L) azelastine, M) ritonavir, N) celecoxib, O) nelfinavir, P) praziquantel, Q) lemborexant, R) Inhibitor N3, S) TG-0205221, T) niclosamide, and U) chloroquine.

that of other CoV proteinases. SARS-CoV2 M^{pro} is built in a homodimer conformation, formed of three domains: domains 1 (residues 8–101) and 2 (residues 102–184) are β-barrels, and domain 3 (residues 201–306) comprises mainly α-helices, and it is connected to domain 2 by an elongated loop region (residues 185–200). The substrate-binding site of SARS-CoV2 M^{pro} is situated in a cleft between domain 1 and domain 2. Inhibitor N3 was developed using theoretical methods and it can specifically inhibit M^{pro} from multiple coronaviruses, including SARS-CoV, SARS-CoV2 and MERS-CoV [6–11]. Inhibitor N3 is stabilized at the substrate binding site in an extended conformation by conserved residues (H41 and C145) involved in the catalytic activity of the enzyme, in a similar manner to that observed for other CoV proteinases [4]. The backbone atoms of inhibitor form an antiparallel sheet with some residues of the long strand (residues 155–168), and with residues 189–191 of the loop that connects domain 2 to domain 3.

Proteases are typical targets for drug development because of their recognized enzymatic mechanism, however, many new potential drugs have been ineffective either because of a lack of ligand specificity or because of our incomplete understanding of the conformational state under a biological context of the targeted protease [12]. In order to successfully develop or identify new protease inhibitors, it is necessary to understand important structural features of the protease functions to expand the platform of inhibitor development. Although previous studies have considered the monomeric state of SARS-CoV M^{pro} or SARS-CoV2 M^{pro} to search for new inhibitors [5,13] or to understand the molecular basis of inhibitor recognition [4], kinetic studies have indicated that the active form of the SARS CoV main proteinase corresponds to a homodimer [14], suggesting significant conformational differences between the monomer and dimeric states and indicating that drug discovery combining docking and MD simulations should be performed using the homodimeric conformation instead of the monomer. In the present research, the crystallographic dimeric structure of SARS-CoV2 M^{pro}, the first released structure of this enzyme available at the protein data bank (PDB ID: 6LU7), was docked against 15 Food and Drug Administration (FDA) approved drugs identified in a previous study [5] and then submitted to MD

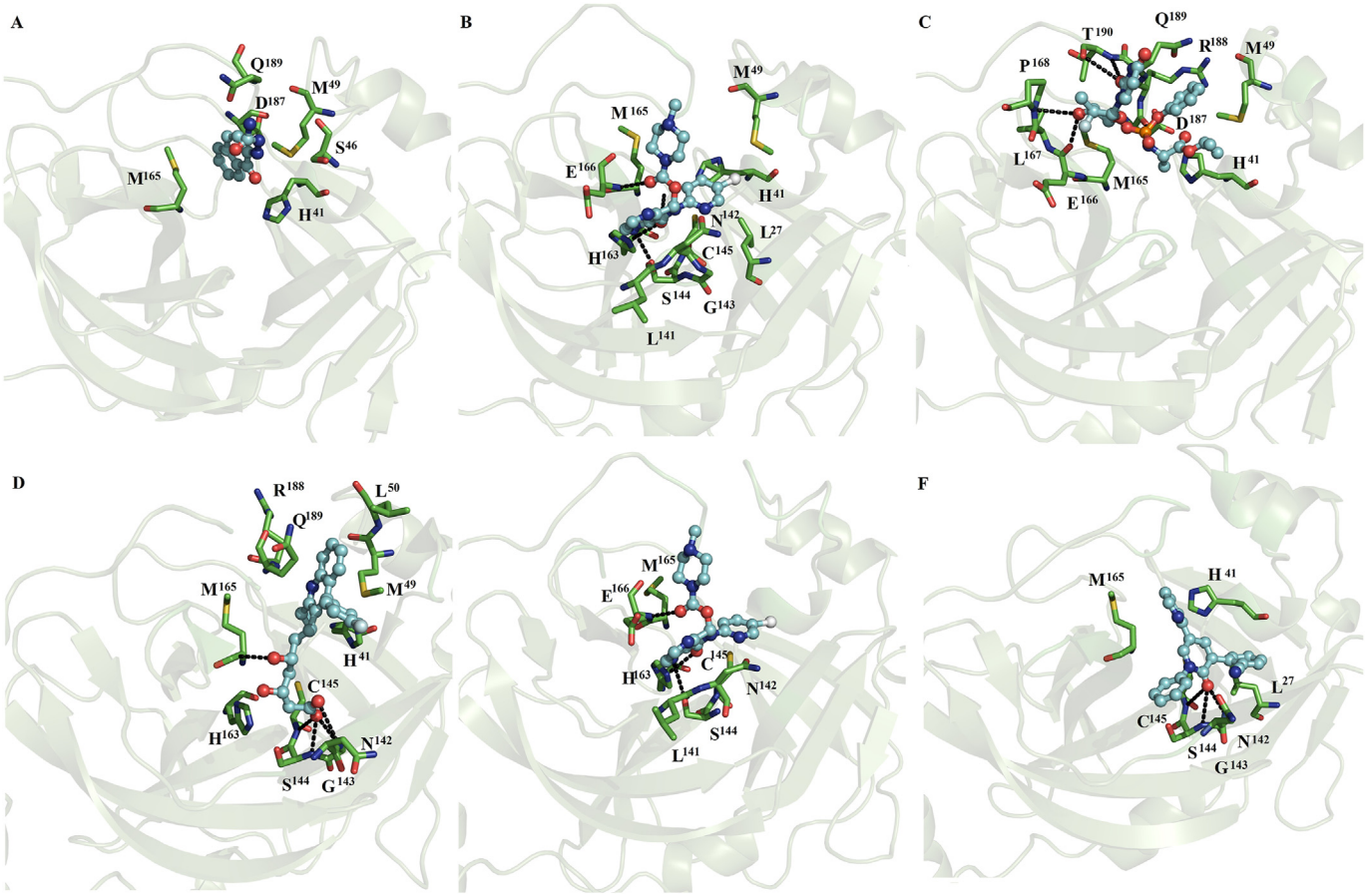

Fig. 1. Binding conformation of complexes between ligands and monomeric SARS-CoV2 M^{pro}. Maps of the interaction of monomeric SARS-CoV2 M^{pro} with naftazone (A), zopiclone (B), sofosbuvir (C), pitavastatin (D), eszopiclone (E), and perampanel (F). Each complex corresponds to the most populated conformation obtained thorough MD simulation. The receptor is represented in a green cartoon representation, the interacting residues are depicted in green sticks, and the ligand is shown in a ball and stick representation. The figure was built with PyMOL [25]. (For interpretation of the references to colour in this figure legend, the reader is referred to the Web version of this article.)

simulations coupled to the MM/GBSA approach to dissect the structural and energetic basis of molecular recognition considering the monomeric and dimeric states. In addition, comparative analysis was performed for dimeric SARS-CoV2 M^{pro} and SARS-CoV M^{pro} coupling to lopinavir and ritonavir, which have been shown to be an effective therapy against SARS-CoV M^{pro}.

2. Methods

2.1. Starting data and preparation systems

Seventeen FDA-approved small drugs (Scheme 1), indomethacin (DB00328), naftazone (DB13680), ofloxacin (DB01165), zopiclone (DB01198), sofosbuvir (DB08934), pitavastatin (DB08860), eszopiclone (DB00402), perampanel (DB08883), fenoterol (DB01288), azelastine (DB00972), celecoxib (DB00482), nelfinavir (DB00220), praziquantel (DB01058), ondansetron (DB00904), lemborexant (DB11951), lopinavir (DB01601) and ritonavir (DB00503), were downloaded from DrugBank version 5.0 [15] and optimized at the AM1 level employing Gaussian 09 W [16]. The X-ray crystallography structures of SARS-CoV2 M^{pro} (PDB ID: 6LU7, 2.16 Å) and SARS-CoV M^{pro} (PDB ID: 2GX4, 1.93 Å) were used to construct the protein-ligand complexes. PDB structures employed for this research were selected based on their availability (PDB ID: 6LU7, 2.16 Å), high resolution, without mutations and missing residues.

2.2. Molecular docking

The seventeen FDA-approved small drugs were docked on monomeric and dimeric SARS-CoV2 M^{pro} using AutoDock Tools 1.5.6 and AutoDock 4.2 programs [17]. Lopinavir and ritonavir were docked on monomeric and dimeric SARS-CoV M^{pro}. In the previous docking calculation, hydrogen atoms were added to the ligand, and protein atoms and Kollman and Gasteiger partial charges were assigned for the receptor and ligand, respectively. The grid box was centered on the substrate-binding site of each monomeric subunit with grid points in the x, y and z of 70 × 70 × 70 Å, respectively, with a grid spacing of 0.375 Å. The ligand place was optimized using a Lamarckian genetic algorithm. The protein-ligand conformation with the lowest binding energies was selected as the initial conformer to start MD simulations. The compounds reached the substrate binding site of SARS-CoV M^{pro} and SARS-CoV2 M^{pro}, obtaining a root-mean-square deviation (RMSD) of 0.5 Å to 2.0 Å with respect to the co-crystallized compound. About 20 runs were run for each compound and 30 binding poses of the ligand were obtained between compounds and receptor. The docking protocol was validated by reproducing the experimental binding mode of inhibitor N3 and TG-0205221 (scheme) on SARS-CoV2 M^{pro} (PDB ID: 6LU7) and SARS-CoV M^{pro} (PDB ID: 2GX4), respectively. By using this methodology, we identified that our docking methodology was able to reproduce the experimental binding mode of both compounds with RMSD values lower than 1.0 Å.

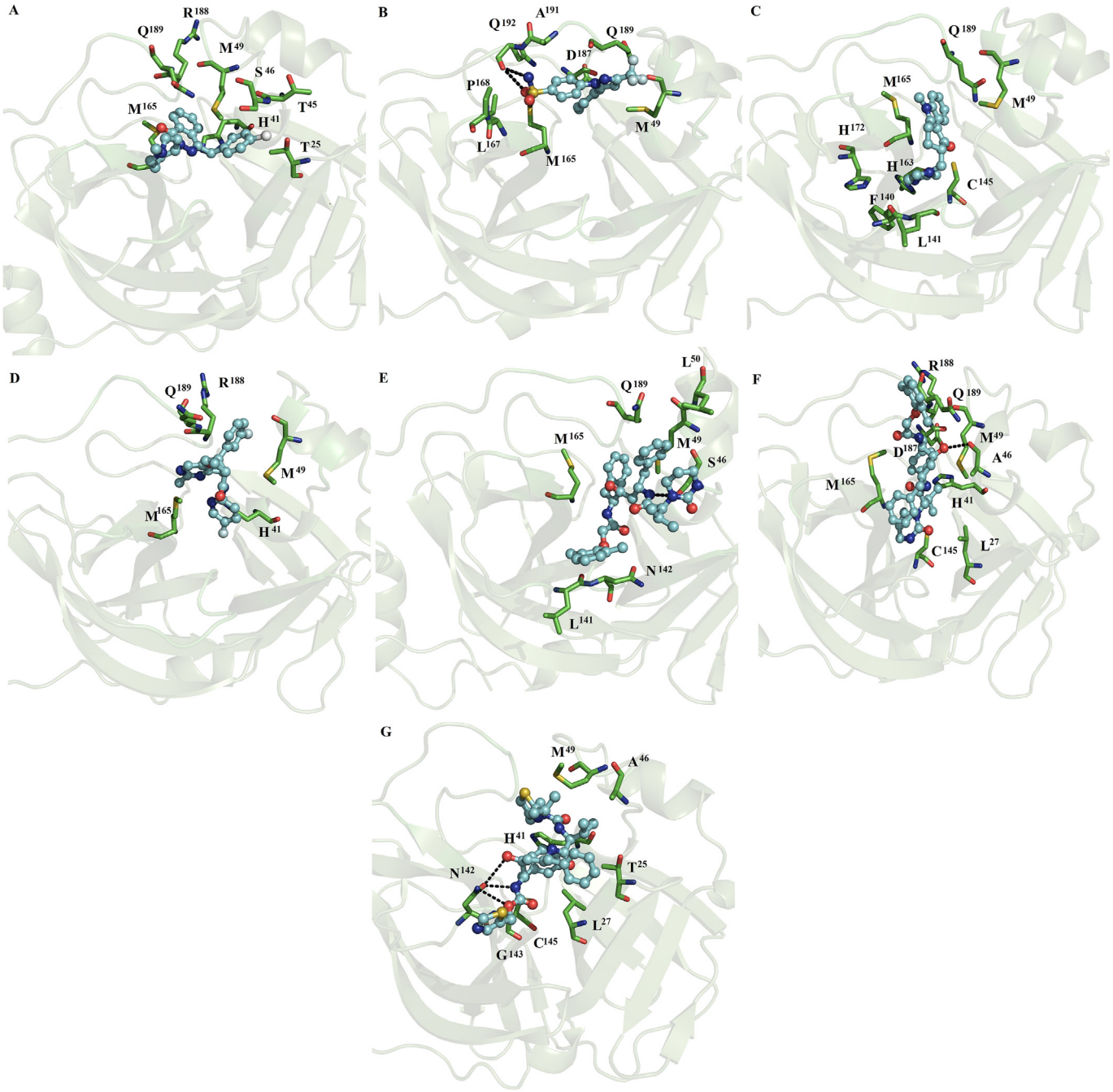

Fig. 2. Binding conformation of complexes between ligands and monomeric SARS-CoV2 M^{pro} and SARS-CoV M^{pro}. Diagrams of the interaction of complexes of monomeric SARS-CoV2 M^{pro} with azelastine (A), celecoxib (B), ondansetron (C) and lemborexant (D) and lopinavir (E). Diagrams of the interaction of monomeric SARS-CoV M^{pro} with lopinavir (F) and ritonavir (G).

2.3. MD simulations

MD simulations were carried out using the AMBER16 package [18] and the ff14SB force field [19]. The force field of ligands was performed considering AM1-BCC atomic charges and the general Amber force field (GAFF) [20]. Each complex generated through docking was neutralized with 0.10 M NaCl and then solvated using the TIP3P water model [21] in a dodecadic box of 12.0 Å. Previously, MD simulations for each complex were minimized through 1000 steps for the steepest descent and 3000 steps for the conjugate gradient. Then, the systems were heated through 200 ps, the density was equilibrated through 200 ps, and finally, the systems were equilibrated by 600 ps of constant pressure equilibration at 310 K. Once the systems were equilibrated, MD simulations were run for 100 ns with triplicate experiments using an NPT ensemble at 310 K. The electrostatic forces were described by the particle mesh Ewald method [22], and a 10 Å cutoff was chosen for the van der Waals interactions. The SHAKE algorithm [23] was used to constrain bond lengths at their equilibrium values. Temperature and pressure were maintained using the weak-coupling algorithm [24]. The results were analyzed using AmberTools16. Images were built using PyMOL [25].

2.4. Binding free energy and per-residue decomposition calculations

The MM/GBSA [26,27] method was employed to calculate the binding free energy (ΔG_{bind}) values between the receptor and ligand and to calculate per-residue decomposition analysis. To this end, 500 snapshots at time intervals of 100 ps were selected over the equilibrated time, removing all counterions and water molecules with a salt concentration of 0.10 M [28]. ΔG_{bind} and per-residue decomposition calculations were determined as described elsewhere [29], and the ΔG_{bind} values represent the average values of triplicate simulation experiments. Similar experiments were performed using compounds with known experimental affinity to SARS-CoV2 M^{pro} or SARS-CoV M^{pro} to validate the ability of MM/GBSA approach to reproduce the experimental binding affinity trend. We observed that the approach was able to reproduce the experimental tendency previously observed for two inhibitors (Chloroquine and niclosamide) of SARS-CoV2 M^{pro} [30], for which niclosamide showed higher affinity for SARS-CoV2 M^{pro} in comparison to chloroquine (supplementary material, Table S1). Similarly, TG-0205221, a SARS-CoV M^{pro} inhibitor, showed a higher affinity for SARS-Cov M^{pro} (supplementary material, Table S1) in comparison to lopinavir (Table 2), in line with experimental reports [31,32].

3. Results and discussion

3.1. Docking between ligands and monomeric SARS-CoV2 M^{pro}

Docking studies between ligands and SARS-CoV2 M^{pro} showed that all ligands: indomethacin (Fig. S1A), naftazone (Fig. S1B), ofloxacin (Fig. S1C), zopiclone (Fig. S1D), sofosbuvir (Fig. S1E), pitavastatin (Fig. S1F), eszopiclone (Fig. S2A), perampanel (Fig. S2B), fenoterol (Fig. S2C), azelastine (Fig. S2D), celecoxib (Fig. S2E), nelfinavir (Fig. S2F), praziquantel (Fig. S3A), ondansetron (Fig. S3B), and lemborexant (Fig. S3C) reached the catalytic binding site of SARS-CoV2 M^{pro} (supplementary material, Figs. S1–S3 and Table S2). These ligands were mostly stabilized by H41, F140, N142, C145, H163, H164, M165, E166, Q189 and R188 residues through nonpolar interactions. H41, S46, Y54, F140, L141, N142, G143, S144, C145, H163, H164, E166 and D187 established polar interactions through backbone or side chain atoms with some of the compounds: indometachin (Fig. 1A), naftazone (Fig. S1B), ofloxacin (Fig. S1C), zopiclone (Fig. S1D), sofosbuvir (Fig. S1E), pitavastatin (Fig. S1F), perampanel (Fig. S2B), fenoterol (Fig. S2C), azelastine (Fig. S2D), praziquantel (Fig. S3A), ondansetron (Fig. S3B), lemborexant (Fig. S3C), and ritonavir (Fig. S3E). The residues stabilizing the ligands were mostly distributed between domains 1 (residues 8–101) and 2 (residues 102–184), and the interactions established were similar to those observed in the co-crystallized complex

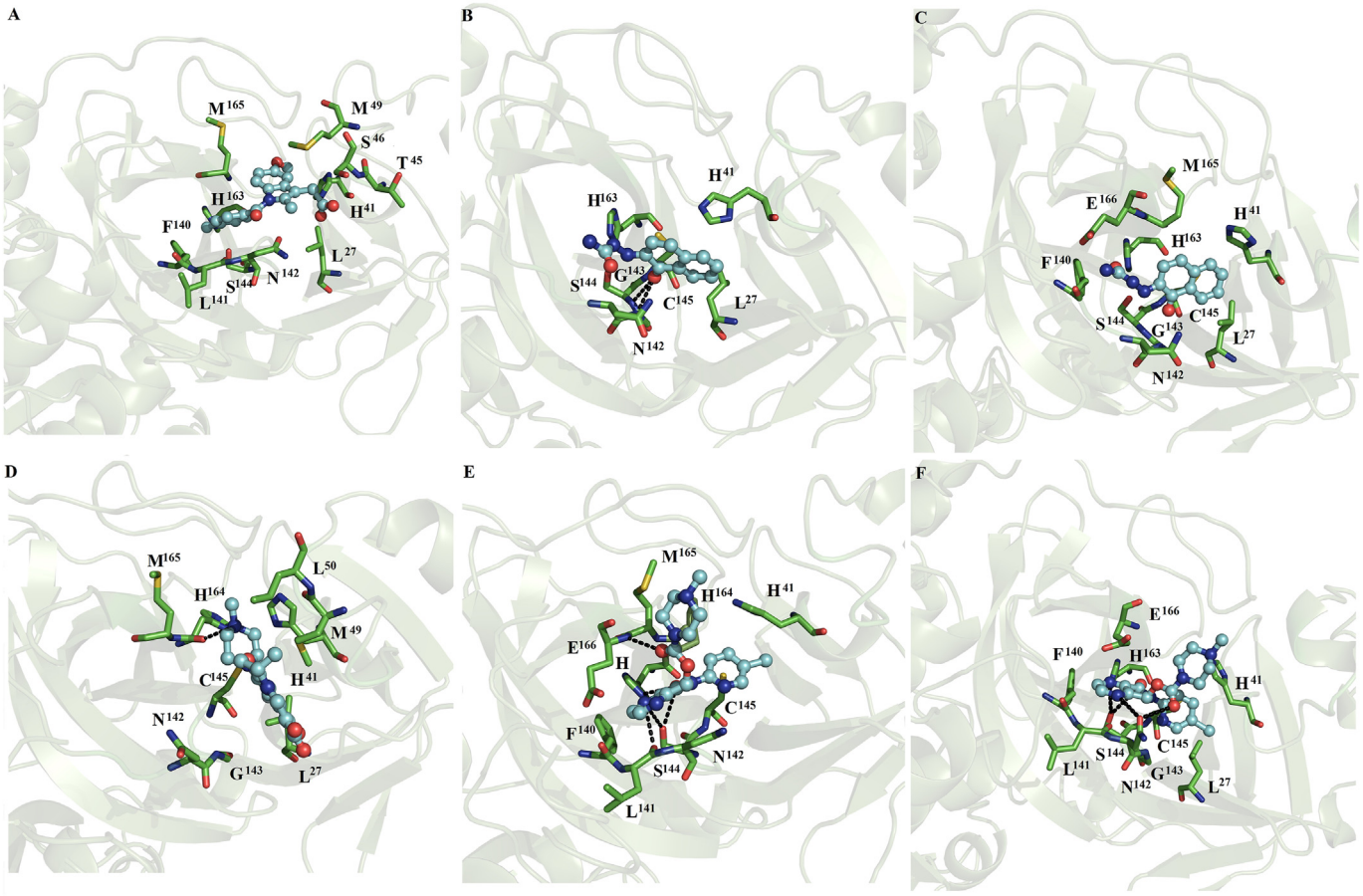

Fig. 3. Binding conformation of complexes of ligands with dimeric SARS-CoV2 M^{pro}. Indomethacin coupled to subunit 2 (A), naftazone bound to subunits 1 (B) and 2 (C), ofloxacin bound to subunit 1 (D), and zopiclone coupled to subunits 1 (E) and 2 (F) of dimeric SARS-CoV2 M^{pro}.

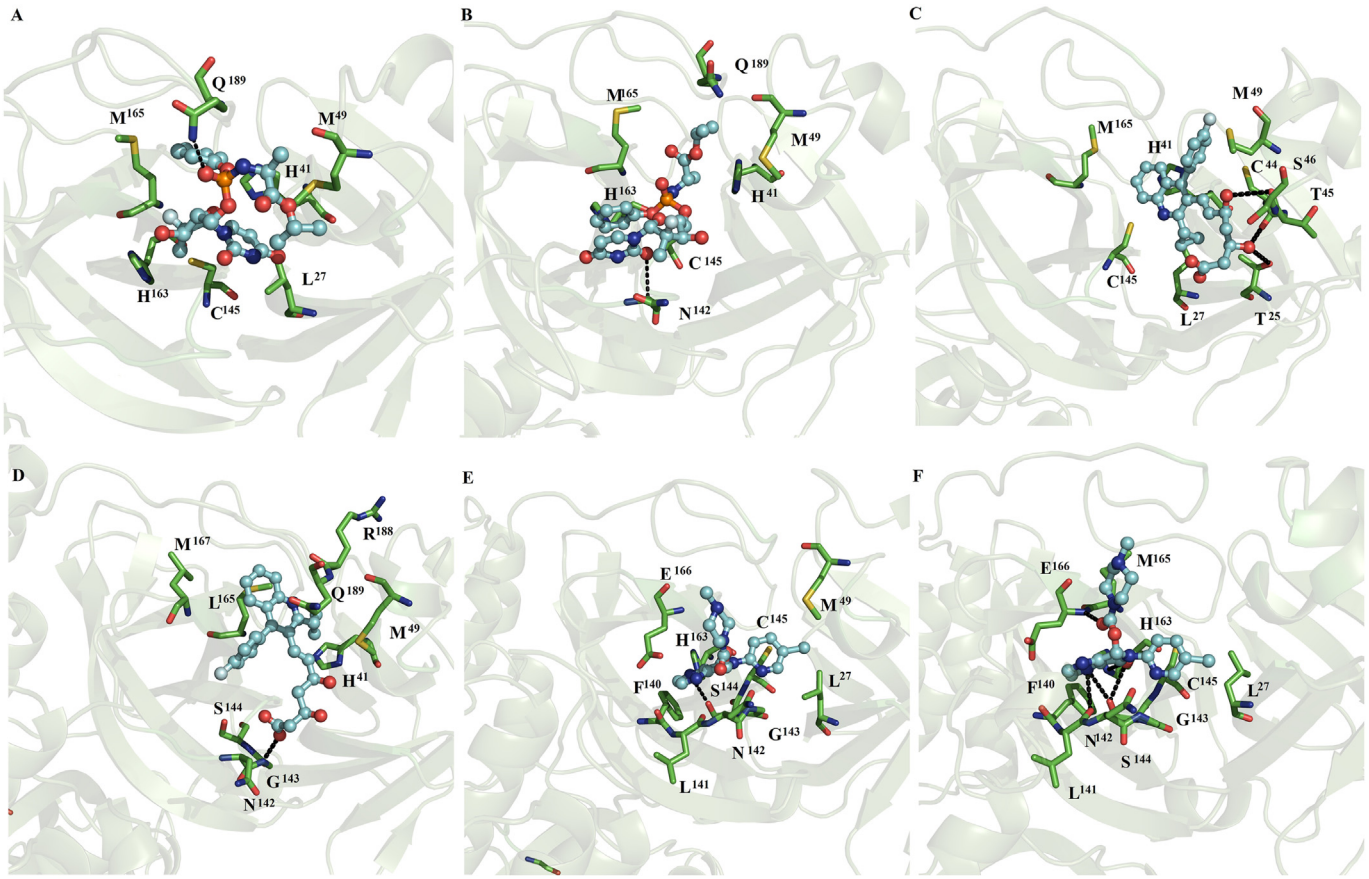

Fig. 4. Binding conformation of complexes of ligands with dimeric SARS-CoV2 M^{pro}. Sofosbuvir bound at subunits 1 (A) and 2 (B), pitavastatin bound at subunits 1 (C) and 2 (D), and eszopiclone bound at subunits 1 (E) and 2 (F) of dimeric SARS-CoV2 M^{pro}.

between the SARS-CoV2 M^{pro} ligand and the inhibitor N3 (PDB ID: 6LU7), highlighting the interactions with conserved residues (H41 and C145) involved in the catalytic activity of the enzyme [33].

3.1.1. Docking of lopinavir or ritonavir with monomeric SARS-CoV2 M^{pro} and SARS-CoV M^{pro}

Docking studies show that lopinavir and ritonavir on SARS-CoV2 M^{pro} and SARS-CoV M^{pro} reached the catalytic site of both systems (supplementary material, Figs. S3D–G and Table S2). On SARS-CoV2, lopinavir (Fig. S3D) and ritonavir (Fig. S3E) were mostly stabilized by T25, T26, H41, F140, L141, N142, G143, H163, E166, D187, Q189 and R188 residues through nonpolar interactions, whereas ritonavir established polar interactions with the side chain of S46 (Fig. S3E). On SARS-CoV M^{pro}, lopinavir (Fig. S3F) and ritonavir (Fig. S3G) are mostly stabilized by T25, A46, M49, L141, S144, E166 and Q189 through nonpolar interactions, while ritonavir formed polar interactions with the side chain of Q189 (Fig. S3G).

Comparative analysis between the coupling of lopinavir or ritonavir on SARS-CoV2 M^{pro} and SARS-CoV M^{pro} showed that T25, S/A46, Y/M49, L141, S144, E166 and Q189 are present in the stabilization of ligands on SARS-CoV2 M^{pro} and SARS-CoV M^{pro}. In addition, these compounds are better stabilized on SARS-CoV2 M^{pro} than on SARS-CoV M^{pro}. All these docking-predicted complexes were submitted to MD simulation in the monomeric and dimeric states to validate their stabilization at the catalytic sites of SARS-CoV2 M^{pro} and SARS-CoV M^{pro}.

3.2. Convergence of MD simulations

RMSD and radius of gyration (Rg) studies showed that monomeric SARS-CoV2 M^{pro} and SARS-CoV M^{pro} in their free and bound states reached equilibrium between 10 and 20 ns with average values that oscillated between 1.6 ± 0.2 and 3.8 ± 0.2 Å for RMSD and 21.9 ± 0.2 and 23.1 ± 0.2 Å for R_G (Table S3, supplementary material). Dimeric SARS-CoV2 M^{pro} and SARS-CoV M^{pro} in their free and bound states reached equilibrium among 10–30 ns with average values that ranged between 1.5 ± 0.1 and 2.2 ± 0.2 Å for RMSD and 25.8 ± 0.2 and 26.1 ± 0.2 Å for R_G (Table S4, supplementary material). Therefore, for further analyses, the first 30 ns were discarded from the 100 ns simulation for each monomer and dimer simulations.

3.3. MD simulations of ligands with monomeric SARS-CoV2 M^{pro} and SARS-CoV M^{pro}

MD simulations show that indomethacin, ofloxacin, fenoterol, nelfinavir, praziquantel and ritonavir lost interactions at the catalytic site of SARS-CoV2 M^{pro}. In contrast, naftazone (Fig. 1A), zopiclone (Fig. 1B), sofosbuvir (Fig. 1C), pitavastatin (Fig. 1D), eszopiclone (Fig. 1E), perampanel (Fig. 1F), azelastine (Fig. 2A), celecoxib (Fig. 2B), ondansetron (Fig. 2C), and lemborexant (Fig. 2D) maintained interactions with the catalytic site of SARS-CoV2 M^{pro}. These compounds were mainly stabilized by M49, M165 and Q189 residues through nonpolar interactions. However, S46, G143, S144, H163, M165, C145, E166, P168, D187, T190 and Q192 formed polar interactions with backbone or side chain atoms with some of the

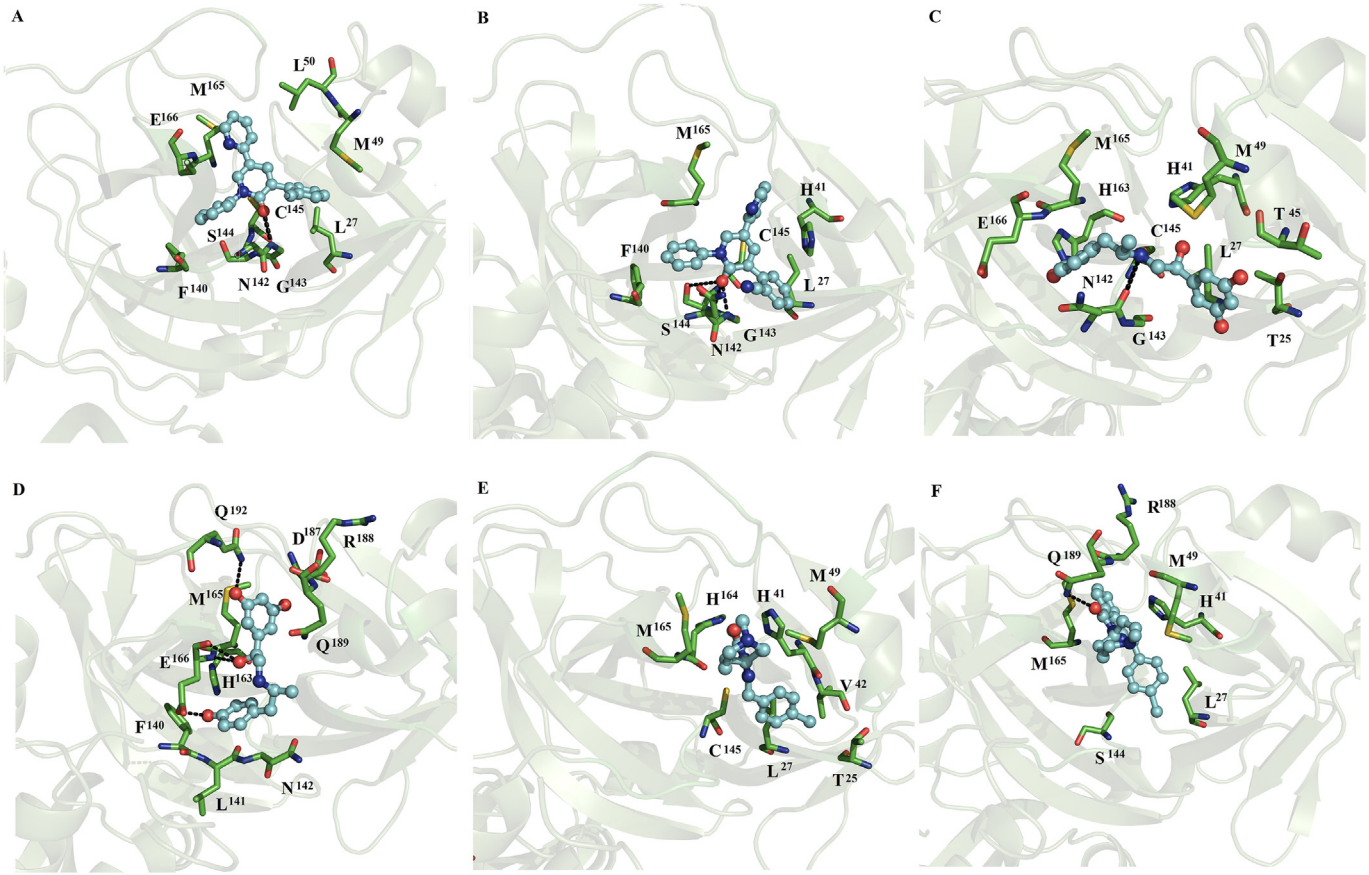

Fig. 5. Binding conformation of complexes of ligands with dimeric SARS-CoV2 M^{pro}. Perampanel bound at subunits 1 or 2 (A and B), fenoterol bound at subunits 1 or 2 (Fig. C and D), and azelastine bound at subunits 1 and 2 (Fig. E and F) of dimeric SARS-CoV2 M^{pro}.

compounds, including naftazone (Fig. 1A), zopiclone (Fig. 1B), T190 (Fig. 1C), pitavastatin (Fig. 1D), eszopiclone (Fig. 1E), perampanel (Fig. 1F), azelastine (Fig. 2A), celecoxib (Fig. 2B), ondansetron (Fig. 2C), and lemborexant (Fig. 2D).

3.3.1. MD simulations of lopinavir or ritonavir with monomeric SARS-CoV2 M^{pro} and SARS-CoV M^{pro}

MD simulations showed that ritonavir lost interactions with the catalytic site of SARS-CoV2, whereas lopinavir maintained the interactions with the catalytic site (Fig. 2E). Lopinavir was mostly stabilized by hydrophobic residues (M49, M165 and Q189) similar to those present in the fifteen repositioned compounds (Figs. 1 and 2), while it established polar interactions with the side chain of S46 (Fig. 2E). On SARS-CoV M^{pro}, lopinavir and ritonavir were mainly stabilized by L27, H41, A46, M49 and C145 through hydrophobic interactions, whereas lopinavir formed polar interactions with backbone atoms of A46 (Fig. 2F), and ritonavir formed polar interactions with the side chain of N142 (Fig. 2G).

Analyses between the coupling of lopinavir or ritonavir on SARS-CoV2 M^{pro} and SARS-CoV M^{pro} showed that only hydrophobic contacts with M49 were shared in the stabilization of the fifteen repositioned compounds on SARS-CoV2 M^{pro} and SARS-CoV M^{pro}. In addition, the stabilization of these compounds was better on SARS-CoV2 M^{pro} than on SARS-CoV2 M^{pro}.

3.3.2. MD simulations of ligands with dimeric SARS-CoV2 M^{pro} and SARS-CoV M^{pro}

In contrast, with the observations with monomeric SARS-CoV2 and SARS-CoV M^{pro}, MD simulations for most of the dimeric systems showed that all the ligands remained on both subunits of the dimer, except for the complexes between indomethacin, ofloxacin and lemborexant with SARS-CoV2 M^{pro}, in which these compounds only remained at one of the catalytic sites of SARS-CoV2 M^{pro}. Indomethacin coupled to subunit 2 (Fig. 3A), naftazone bound to subunits 1 and 2 (Fig. 3B and C), ofloxacin bound to subunit 1 (Fig. 3D), and zopiclone coupled to subunits 1 and 2 (Fig. 3E and F). Sofosbuvir bound at subunits 1 and 2 (Fig. 4A and B), pitavastatin bound at subunits 1 and 2 (Fig. 4C and D), and eszopiclone bound at subunits 1 and 2 (Fig. 4E and F). Perampanel coupled at subunit 1 or 2 (Fig. 5A and B), fenoterol bound at subunit 1 or 2 (Fig. 5C and D), and azelastine bound at subunits 1 and 2 (Fig. 5E and F). Celecoxib coupled at subunits 1 and 2 (Fig. 6A and B), nelfinavir bound at subunits 1 and 2 (Fig. 6C and D), and praziquantel bound at subunits 1 and 2 (Fig. 6E and F). Ondansetron bound at subunits 1 and 2 (Fig. 7A and B), and lemborexant bound at subunit 2 (Fig. 7C). These compounds were mainly stabilized by L27, H41, M49, N142, C145 and M165 through nonpolar interactions. T25, H41, T45, S46, L141, N142, G143, F140, S144, H163, H164, M165, E166, Q192, and Q189 formed polar interactions with backbone or side chain atoms with some of these compounds: naftazone (Fig. 3B), ofloxacin (Fig. 3D), zopiclone (Fig. 3E and F), sofosbuvir (Fig. 4A and B), pitavastatin (Fig. 4C and D), eszopiclone (Fig. 4E and F), perampanel (Fig. 5A and B), fenoterol (Fig. 5C and D), azelastine (Fig. 5F), celecoxib (Fig. 6A and B), nelfinavir (Fig. 6C and D), praziquantel (Fig. 6E and F), ondansetron (Fig. 7A and B) and lemborexant (Fig. 7C). Comparison of the residues stabilizing these ligands in the monomeric (Figs. 1 and 2) versus dimeric SARS-CoV2 M^{pro} and SARS-CoV M^{pro} (Figs. 3 and 7) revealed that the

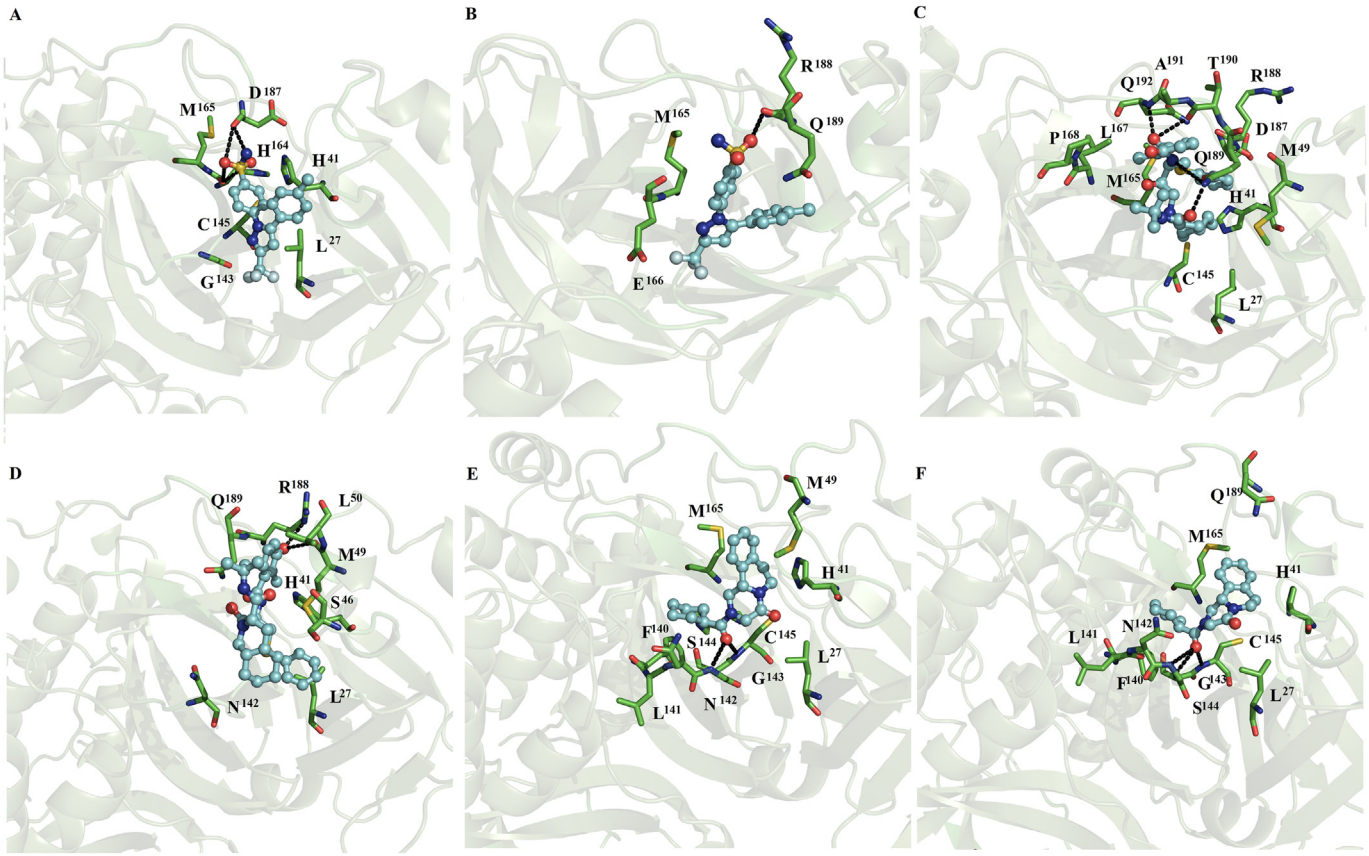

Fig. 6. Binding conformation of complexes of ligands with dimeric SARS-CoV2 M^{pro}. Celecoxib bound at subunits 1 and 2 (A and B), nelfinavir bound at subunits 1 and 2 (Fig. 6C and D), and praziquantel bound at subunits 1 and 2 (Fig. 6E and F) of dimeric SARS-CoV2 M^{pro}.

repositioned compounds were better stabilized in the dimeric state than in the monomeric state. In addition, only in the complexes using the dimeric system, the presence of interactions with conserved residues (H41 and C145) involved in the catalytic activity was observed [33].

3.3.3. *MD simulations of lopinavir or ritonavir with dimeric SARS-CoV2 M^{pro} and SARS-CoV M^{pro}*

MD simulations showed that lopinavir at subunits 1 (Figs. 7D) and 2 (Fig. 7E) and ritonavir at subunits 1 (Figs. 7F) and 2 (Fig. 8A) were maintained interactions at the catalytic site of SARS-CoV2. Ritonavir and lopinavir were generally stabilized by four residues (M49, M165, L167 and Q189), whereas only lopinavir formed polar interactions with backbone atoms and side chain atoms of T90 and Q189 (Fig. 7E). On SARS-CoV M^{pro}, lopinavir coupled at subunits 1 (Figs. 8B) and 2 (Fig. 8C) and ritonavir coupled at subunit 1 (Fig. 8D) were mostly stabilized by H41, M49, M165 and Q189 through hydrophobic interactions. Similar nonpolar and polar interactions were observed for the fifteen repositioned compounds (Figs. 3–7), except for L167. Comparative analysis of the residues stabilizing ritonavir and lopinavir in the monomeric (Fig. 2) versus dimer SARS-CoV2 M^{pro} and SARS-CoV M^{pro} (Figs. 7 and 8) showed that ritonavir is stabilized by similar hydrophobic residues (M49 and M165) in the monomeric and dimeric states, whereas only two residues (H41 and M49) are shared in the stabilization of lopinavir in the monomeric and dimeric SARS-CoV2 M^{pro} and SARS-CoV M^{pro}.

3.4. *Binding free energy calculations*

Differences in affinity for the complexes between ligands and monomeric and dimeric SARS-CoV2 M^{pro} and SARS-CoV M^{pro} systems were calculated using the MM/GBSA approach, showing that all the bindings are energetically favorable and guided through nonpolar interactions, van der Waals energy (ΔE_{vdw}) and the nonpolar free energy of desolvation ($\Delta G_{npol,sol}$). Binding free energy (ΔG_{bind}) values for the ligands coupled at the monomeric SARS-CoV2 M^{pro} show the following tendency: perampanel > lopinavir > ondansetron > pitavastatin > zopiclone > azelastine > sofosbuvir = eszopiclone > celecoxib > lemborexant (Table 1). However, a higher affinity towards monomeric SARS-CoV M^{pro} was exhibited by lopinavir than by ritonavir. Comparison of ΔG_{bind} values for the affinity of repositioned compounds with ritonavir or lopinavir shows that perampanel was able to inhibit monomeric SARS-CoV M^{pro} in a similar manner to lopinavir and ritonavir, which diffuses in the first nanoseconds of MD simulations (see section 3.3.1). Comparisons between the affinity of lopinavir or ritonavir for monomeric SARS-CoV2 M^{pro} and SARS-CoV M^{pro} systems showed that these two compounds exhibit a higher affinity by monomeric SARS-CoV M^{pro} than by SARS-CoV2 M^{pro}.

ΔG_{bind} values for the ligands coupled on the first subunit of dimeric SARS-CoV2 M^{pro} show the following tendency: perampanel > lopinavir > praziquantel > ritonavir > ofloxacin > azelastine > zopiclone > eszopiclone > fenoterol > pitavastatin > nelfinavir = celecoxib > sofosbuvir > ondansetron > naftazone. The ligands coupled at the second subunit showed the following order: nelfinavir > lopinavir > praziquantel > perampanel

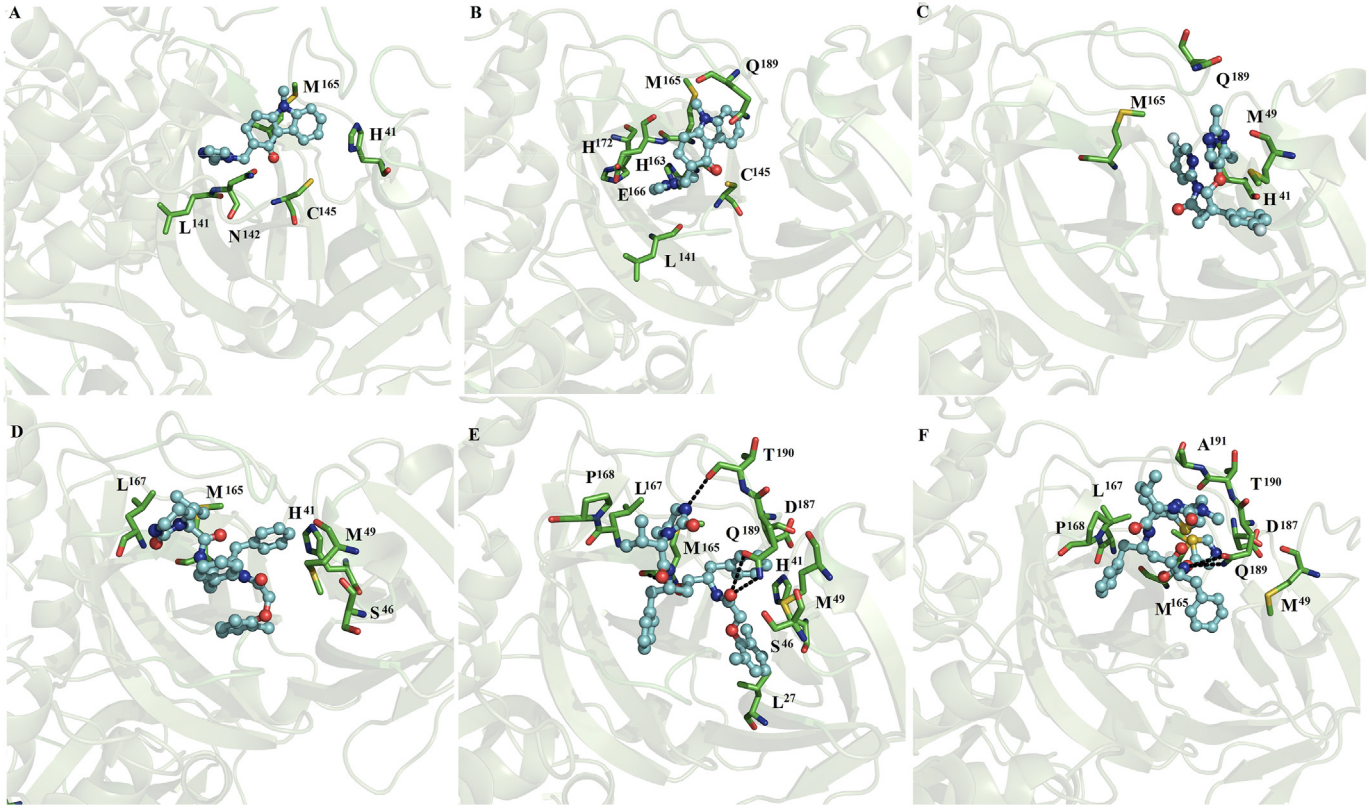

Fig. 7. Binding conformation of complexes of ligands with dimeric SARS-CoV2 M^{pro}. Ondansetron bound at subunits 1 and 2 (A and B), lemborexant bound at subunit 2 (C), lopinavir at subunits 1 (D) and 2 (E) and ritonavir at subunit 1 (F) of dimeric SARS-CoV2 M^{pro}.

> azelastine > ritonavir > eszopiclone > fenoterol > ondansetron > pitavastatin > zopiclone > sofosbuvir > celecoxib > lemborexant > indomethacin > naftazone (Table 2). Based on this analysis, it is evident that perampanel, and praziquantel can be proposed as anti-COVID-19 clinical drugs, whereas nelfinavir could also exhibit moderate activities against COVID-19. Perampanel is a drug currently employed in epilepsy, with an innovative mechanism of action through AMPA ([2-amino-3- (3-hydroxy-5-methyl-isoxazol-4-yl) propanoic acid) glutamate receptors. Praziquantel is an anthelmintic drug used to treat several sorts of parasitic worm infections, and nelfinavir is a strong HIV1 protease inhibitor used with other antiviral medications to treat HIV. Interestingly, perampanel and praziquantel also exhibit a similar affinity to lopinavir and a higher affinity than ritonavir, both known inhibitors of SARS-CoV M^{pro} [3]. A comparison of the ΔG_{bind} values of lopinavir and ritonavir on dimeric SARS-CoV M^{pro} versus SARS-CoV2 M^{pro} indicated that these compounds exhibit a higher affinity for dimeric SARS-CoV2 M^{pro} than for SARS-CoV2 M^{pro}. In addition, a comparison between the monomeric versus dimeric SARS-CoV2 M^{pro} and SARS-CoV M^{pro} systems shows that although the employment of the monomeric system allowed us to identify perampanel and lopinavir as good inhibitors of SARS-CoV2, it did not permit to the identification with praziquantel nelfinavir and ritonavir, highlighting the suitability of employing the dimeric system for drug discovery.

3.5. Per-residue free energy decomposition

An analysis of the residues contributing to the ΔG_{bind} values for complexes with monomeric and dimeric SARS-CoV2 M^{pro} and SARS-CoV M^{pro} systems resulted in 5–11 residues (Tables 3–6). An analysis of the residue stabilizing complexes between ligands and monomeric SARS-CoV2 M^{pro} and SARS-CoV M^{pro} systems showed that H41, M49, M165 and Q189 were present in most of the complexes (Table 3), but only H41 and M165 were present for perampanel, the compound with the highest affinity for monomeric SARS-CoV2 (Table 1); instead, it was stabilized by N142, G143, S144 and C145, which together with M165, contributed the most to the ΔG_{bind} value. M49 and M165 were present in the stabilization of lopinavir, the second-best compound, in the monomeric SARS-CoV2 M^{pro} and SARS-CoV M^{pro} systems.

For the dimeric SARS-CoV2 M^{pro} and SARS-CoV M^{pro} systems, H41, M49 and M165 were present in the stabilization of almost all the complexes (Tables 4–6). From these three residues, the energetic contribution of H41 and M49 was only present in one of the subunits for the complex between dimeric SARS-CoV2 M^{pro} and perampanel (Table 5). H41 was present in both subunits of the complex between SARS-CoV2 M^{pro} and praziquantel, and M49 was present only in subunit 1 for perampanel (Table 5). H41 and M49 were present in the complexes of dimeric SARS-CoV2 M^{pro} with nelfinavir (Table 5) and lopinavir (Table 6). M49 was present in the complex of dimeric SARS-CoV2 M^{pro} with ritonavir (Table 6).

As observed for the complex between perampanel and monomeric SARS-CoV2 M^{pro} (Table 3), N142, G143, S144 and C145, together with M165, contributed the most to the ΔG_{bind} value (Table 2) on both subunits of dimeric SARS-CoV2 M^{pro} (Table 5). For praziquantel, the energetic contribution of M49 was only observed for one of the subunits, whereas participation of H41 and M165 was observed for both subunits, and as observed for perampanel, in which N142, G143, S144, C145 and M165 contributed importantly to the ΔG_{bind} value (Table 2). For nelfinavir, the participation of H41, M49 and M165 was seen only in one of the subunits, the one with

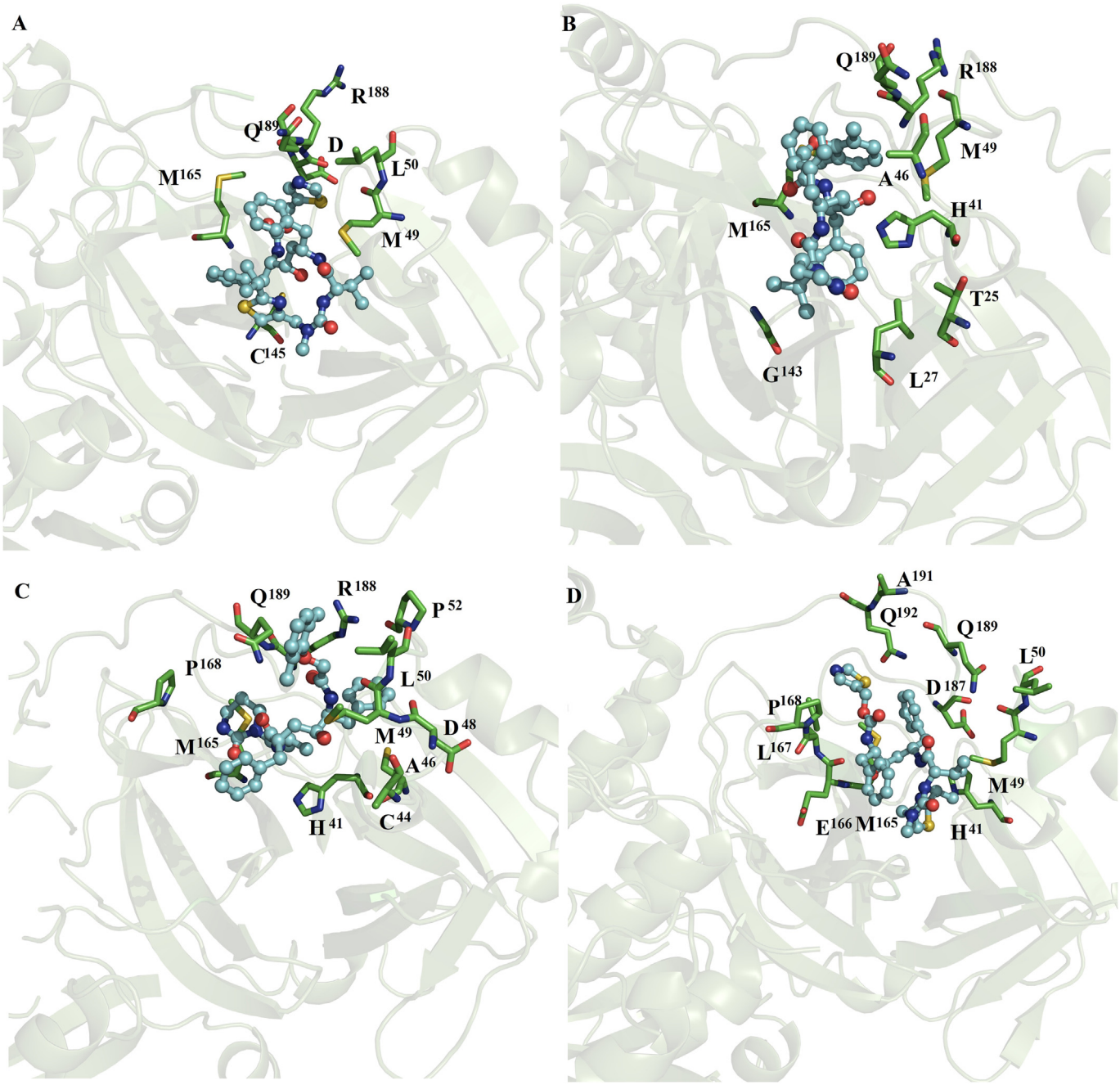

Fig. 8. Binding conformation of complexes of ligands with dimeric SARS-CoV2 and SARS-CoV M^{pro}. Ritonavir bound at subunit 2 (A) of dimeric SARS-CoV2 M^{pro}. Lopinavir coupled at subunits 1 (B) and 2 (C) and ritonavir at subunit 1 (D) of dimeric SARS-CoV M^{pro}.

the higher affinity (Table 2), where it was also observed for the energetic contribution of D187, Q189, T190, A191 and Q192, which contributed importantly to the ΔG_{bind} value (Table 2). Energetic contributions of H41, M49 and M165 residues were observed for complexes of lopinavir with the dimeric SARS-CoV2 M^{pro} and SARS-CoV M^{pro} (Table 6). Significant participation of P168, D187, Q189 and T190 was also observed but only for interactions at subunit 2 of the dimeric SARS-CoV2 M^{pro} in complex with lopinavir (Table 6), whereas Q189 contributed importantly to the ΔG_{bind} value in both subunits of the dimeric SARS-CoV M^{pro} (Table 6).

Energetic contributions of M49 and M165 were observed for complexes of ritonavir with dimeric SARS-CoV2 M^{pro} and of H41 M49 and M165 with dimeric SARS-CoV M^{pro} (Table 6). It was also observed that there was significant participation of P168, Q189 and A191 for interactions of ritonavir at subunit 1 of dimeric SARS-CoV2 M^{pro} and of D166, L167, P168, and Q189 for ritonavir at subunit 1 of dimeric SARS-CoV M^{pro}. Overall, this analysis supports the importance of two conserved residues (H41 and C145) [4] in the stabilization of different inhibitors and highlights the importance of other residues (M49, N142, G143, S144, M165, D187, Q189, T190, A191 and Q192) in ligand stabilization. The identification of these 12 hot-spot residues allow to explain the differences in ligand affinity in the monomeric, dimeric and between each subunit of dimer. Although these residues do not form part of the protein-protein interface: domain 1 (residues 10–11 and14), domain 2 (122–127, 137–141, 166, 170 and 172) and domain 3 (280, 283, 285, 286, 290,

Table 1
Binding free energy components for complexes between ligands and monomeric SARS-CoV2 M^{pro} and SARS-CoV M^{pro} systems (in units of kcal/mol).

System	ΔE_{vdw}	ΔE_{ele}	$\Delta G_{ele,sol}$	$\Delta G_{npol,sol}$	DG_{mmgbsa}
SARS-CoV2					
Naftazone	−22.4 ± 2.7	−5.5 ± 1.0	15.8 ± 5.0	−2.9 ± 0.30	−15.0 ± 3.0
Zopiclone	−38.0 ± 2.5	−127.0 ± 11.0	141.0 ± 5.0	−3.9 ± 0.30	−27.9 ± 3.0
Sofosbuvir	−37.5 ± 4.0	−22.0 ± 5.0	37.0 ± 4.0	−4.5 ± 0.4	−27.0 ± 3.0
Pitavastatin	−35.0 ± 5.0	6.7 ± 2.0	4.9 ± 1.0	−4.8 ± 0.3	−28.2 ± 5.0
Eszopiclone	−37.0 ± 2.0	−109.0 ± 10.0	123.0 ± 10.0	−4.0 ± 0.3	−27.0 ± 3.0
Perampanel	−39.0 ± 3.0	−27.0 ± 5.0	39.0 ± 5.0	−4.0 ± 0.2	−31.0 ± 3.0
Azelastine	−36.0 ± 3.0	−107.0 ± 15.0	120.0 ± 14.0	−4.3 ± 0.3	−27.3 ± 3.0
Celecoxib	−31.0 ± 3.0	−11.0 ± 4.0	25.0 ± 3.0	−4.3 ± 0.4	−21.3 ± 4.0
Ondansetron	−40.0 ± 2.0	−16.0 ± 4.0	31.0 ± 3.0	−4.1 ± 0.2	−29.1 ± 3.0
Lemborexant	−32.0 ± 5.0	−4.0 ± 3.0	19.0 ± 3.0	−4.2 ± 0.5	−21.2 ± 5.0
Lopinavir	−44.0 ± 5.0	−36.0 ± 11.0	56.0 ± 10.0	−5.9 ± 0.5	−29.9 ± 5.0
SARS-CoV					
Lopinavir	−51.0 ± 5.0	−10.0 ± 5.0	33.0 ± 4.0	−7.0 ± 0.6	−35.0 ± 4.0
Ritonavir	−40.0 ± 6.0	−9.0 ± 2.0	28.0 ± 6.0	−5.0 ± 0.8	−26.0 ± 5.0

Table 2
Binding free energy components for complexes between ligands and dimeric SARS-CoV2 M^{pro} and SARS-CoV M^{pro} systems (in units of kcal/mol).

System	ΔE_{vdw}	ΔE_{ele}	$\Delta G_{ele,sol}$	$\Delta G_{npol,sol}$	DG_{mmgbsa}
Dimeric SARS-CoV2 M^{pro}					
$SARS\text{-}CoV2_{sub1\text{-}indomethacin}$	ND	ND	ND	ND	ND
$SARS\text{-}CoV2_{sub2\text{-}indomethacin}$	−31.7 ± 4.0	85.3 ± 11.0	−68.8 ± 10.0	−4.1 ± 0.40	−19.30 ± 3.0
$SARS\text{-}CoV2_{sub1\text{-}naftazone}$	−22.17 ± 4.0	−32.7 ± 11.0	40.47 ± 7.0	−3.0 ± 0.30	−17.40 ± 3.0
$SARS\text{-}CoV2_{sub2\text{-}naftazone}$	−26.38 ± 2.0	−26.2 ± 5.0	36.54 ± 4.0	−3.2 ± 0.20	−19.24 ± 3.0
$SARS\text{-}CoV2_{sub1\text{-}ofloxacin}$	−32.27 ± 4.0	−50.4 ± 11.0	58.0 ± 11.0	−4.0 ± 0.40	−28.67 ± 4.0
$SARS\text{-}CoV2_{sub2\text{-}ofloxacin}$	ND	ND	ND	ND	ND
$SARS\text{-}CoV2_{sub1\text{-}zopiclone}$	−37.88 ± 3.0	−114.0 ± 10.0	130.0 ± 10.0	−3.9 ± 0.40	−25.78 ± 3.0
$SARS\text{-}CoV2_{sub2\text{-}zopiclone}$	−38.40 ± 3.0	−117.5 ± 12.0	134.6 ± 13.0	−3.7 ± 0.30	−25.0 ± 4.0
$SARS\text{-}CoV2_{sub1\text{-}sofosbuvir}$	−34.64 ± 5.0	−20.27 ± 9.0	40.0 ± 8.0	−4.6 ± 0.60	−19.51 ± 5.0
$SARS\text{-}CoV2_{sub2\text{-}sofosbuvir}$	−37.44 ± 5.0	−20.0 ± 9.0	38.1 ± 8.0	−4.6 ± 0.60	−23.94 ± 6.0
$SARS\text{-}CoV2_{sub1\text{-}pitavastatin}$	−36.5 ± 3.0	62.7 ± 22.0	−44.2 ± 10.0	−5.0 ± 0.40	−23.0 ± 5.0
$SARS\text{-}CoV2_{sub2\text{-}pitavastatin}$	−40.4 ± 3.0	46.9 ± 12.0	−27.0 ± 6.0	−4.7 ± 0.30	−25.20 ± 4.0
$SARS\text{-}CoV2_{sub1\text{-}eszopiclone}$	−38.1 ± 4.0	−123.5 ± 14.0	142.2 ± 14.0	−3.9 ± 0.40	−23.30 ± 4.0
$SARS\text{-}CoV2_{sub2\text{-}eszopiclone}$	−41.1 ± 3.0	−154.9 ± 21.0	172.0 ± 22.0	−3.9 ± 0.30	−27.90 ± 3.0
$SARS\text{-}CoV2_{sub1\text{-}perampanel}$	−46.2 ± 3.0	−25.0 ± 4.0	39.1 ± 3.0	−5.6 ± 0.20	−37.70 ± 3.0
$SARS\text{-}CoV2_{sub2\text{-}perampanel}$	−42.6 ± 2.0	−23.9 ± 4.0	39.8 ± 3.0	−5.0 ± 0.20	−31.70 ± 2.0
$SARS\text{-}CoV2_{sub1\text{-}fenoterol}$	−34.3 ± 4.0	−120.8 ± 12.0	136.6 ± 12.0	−4.6 ± 0.50	−23.1 ± 5.0
$SARS\text{-}CoV2_{sub2\text{-}fenoterol}$	−33.4 ± 3.0	−118.8 ± 10.0	129.0 ± 10.0	−4.4 ± 0.20	−27.60 ± 4.0
$SARS\text{-}CoV2_{sub1\text{-}azelastine}$	−34.4 ± 4.0	−106.7 ± 12.0	118.0 ± 12.0	−3.9 ± 0.40	−27.0 ± 3.0
$SARS\text{-}CoV2_{sub2\text{-}azelastine}$	−39.27 ± 3.0	−127.7 ± 15.0	142.0 ± 15.0	−4.63 ± 0.30	−29.6 ± 3.0
$SARS\text{-}CoV2_{sub1\text{-}celecoxib}$	−34.42 ± 3.0	−14.4 ± 3.0	30.9 ± 3.0	−4.7 ± 0.30	−22.62 ± 3.0
$SARS\text{-}CoV2_{sub2\text{-}celecoxib}$	−30.59 ± 4.0	−20.0 ± 4.0	33.0 ± 3.0	−4.54 ± 0.50	−22.13 ± 4.0
$SARS\text{-}CoV2_{sub1\text{-}nelfinavir}$	−34.42 ± 3.0	−14.4 ± 3.0	30.9 ± 3.0	−4.7 ± 0.30	−22.62 ± 3.0
$SARS\text{-}CoV2_{sub2\text{-}nelfinavir}$	−48.73 ± 4.0	−175.06 ± 13.0	184.7 ± 10.0	−5.9 ± 0.30	−44.99 ± 5.0
$SARS\text{-}CoV2_{sub1\text{-}praziquantel}$	−43.60 ± 4.0	−18.01 ± 3.0	31.3 ± 3.0	−4.8 ± 0.30	−35.11 ± 3.7
$SARS\text{-}CoV2_{sub2\text{-}praziquantel}$	−43.60 ± 4.0	−18.01 ± 3.0	31.3 ± 3.0	−4.8 ± 0.30	−35.11 ± 3.7
$SARS\text{-}CoV2_{sub1\text{-}ondansetron}$	−30.0 ± 5.0	−5.77 ± 5.0	20.8 ± 5.0	−3.4 ± 0.50	−18.37 ± 5.0
$SARS\text{-}CoV2_{sub2\text{-}ondansetron}$	−37.9 ± 5.0	−15.13 ± 4.0	30.0 ± 4.0	−3.9 ± 0.50	−26.93 ± 5.0
$SARS\text{-}CoV2_{sub1\text{-}lemborexant}$	ND	ND	ND	ND	ND
$SARS\text{-}CoV2_{sub2\text{-}lemborexant}$	−34.1 ± 4.0	−5.42 ± 4.0	21.6 ± 3.0	−4.5 ± 0.50	−22.42 ± 4.0
$SARS\text{-}CoV2_{sub1\text{-}lopinavir}$	−49.3 ± 4.0	−15.2 ± 5.0	34.9 ± 4.0	−6.2 ± 0.44	−35.80 ± 4.0
$SARS\text{-}CoV2_{sub2\text{-}lopinavir}$	−56.9 ± 4.0	−18.8 ± 6.0	40.6 ± 5.0	−7.2 ± 0.50	−42.30 ± 4.0
$SARS\text{-}CoV2_{sub1\text{-}ritonavir}$	−45.8 ± 5.0	−10.5 ± 4.0	32.5 ± 4.0	−5.5 ± 0.70	−29.30 ± 5.0
$SARS\text{-}CoV2_{sub2\text{-}ritonavir}$	−47.9 ± 6.0	−9.0 ± 3.0	34.2 ± 5.0	−5.8 ± 0.80	−28.50 ± 5.0
Dimeric SARS-CoV2 M^{pro}					
$SARS\text{-}CoV_{sub1\text{-}lopinavir}$	−38.4 ± 4.0	−9.5 ± 5.0	29.9 ± 5.0	−4.7 ± 0.44	−22.70 ± 3.0
$SARS\text{-}CoV_{sub2\text{-}lopinavir}$	−43.7 ± 6.0	−21.7 ± 13.0	40.7 ± 13.0	−5.6 ± 0.80	−30.30 ± 6.0
$SARS\text{-}CoV_{sub1\text{-}ritonavir}$	−49.8 ± 5.0	−22.6 ± 4.0	41.1 ± 4.0	−6.4 ± 0.60	−37.70 ± 5.0
$SARS\text{-}CoV_{sub2\text{-}ritonavir}$	ND	ND	ND	ND	ND

298, 299 and 303), they are in close distance of residues forming the protein-protein interface. Therefore, the ligand binding in dimer is impacted not only by the modulating of these key residues, but also by the induced fit binding of ligand.

3.6. Principal component analysis

PCA was performed to provide a quantified estimation of the differences in mobility. To this end, the trace of the diagonalized covariance matrix of the backbone atomic positional fluctuations was determined for the free and bound SARS-CoV2 M^{pro} and SARS-CoV M^{pro} in the monomeric (Table S5, supplementary material) and dimeric states (Table 7 and Fig. S4, supplementary material). Based on this analysis, the values for free and bound monomeric SARS-CoV2 M^{pro} and SARS-CoV M^{pro} systems suggested that only the binding of sofosbuvir and lopinavir to monomeric SARS-CoV2 M^{pro}

Table 3
Per-residue free energy for complexes between ligands and monomeric SARS-CoV2 M^{pro} and SARS-CoV M^{pro} (values kcal/mol).

Residue	Lig2	Lig4	Lig5	Lig6	Lig7	Lig8	Lig10	Lig11	Lig14	Lig15	Lig16	Lig16*	Lig17*
T25							−0.580						−1.609
L27		−0.645				−0.781						−0.671	−1.031
H41	−0.602	−0.652	−1.345	−0.596		−1.073	−1.206			−1.702		−0.926	−1.512
T45							−0.611						
S46/A46	−0.226						−0.878				−0.877	−1.722	−1.029
M49	−1.403	−0.515	−0.822	−1.527			−2.776	−1.191	−0.563	−1.609	−1.884	−2.241	−1.613
L50				−0.906							1.191		
F140									−0.912				
L141		−0.985			−1.148				−0.634		−0.553		
N142		−1.186		−3.120	−0.945	−2.735					−1.371		−0.631
G143		−0.576		−3.576		−2.144							−0.691
S144		−0.673		−2.172	−0.933	−1.154							
C145		−2.102		−2.645	−2.150	−2.101			−0.511			−0.763	−0.670
H163		−1.514		−0.692	−1.437				−2.590				
M165	−1.563	−2.178	−2.688	−2.987	−1.911	−2.137	−1.619	−1.905	−3.285	−1.720	−1.974	−1.881	
D166		−1.819	−0.761		−2.215								
L167			−0.946					−0.876					
P168			−0.837					−0.590					
P169													
H172									−0.502				
D187	−0.570		−1.356					−0.717				−0.916	
R188			−0.752	−1.253			−0.516			−0.932		−0.513	
Q189	−1.336		−2.542	−1.787			−1.238	−1.279	−1.181	−1.628	−0.919	−2.253	
T190			−1.250										
A191								−1.270					
Q192								−2.243					

Indomethacin = lig1, naftazone = lig2, ofloxacin = lig3, zopiclone = lig4, sofosbuvir = lig5, pitavastatin = lig6, eszopiclone = lig7, perampanel = lig8, fenoterol = lig9, azelastine = lig10, celecoxib = lig11, nelfinavir = lig12, praziquantel = lig13, ondansetron = lig14, lemborexant = lig15, lopinavir = lig16, and ritonavir = lig17. *Denotes complexes between monomeric SARS-CoV M^{pro} with lopinavir (lig16*) and ritonavir (lig17*).

Table 4
Per-residue free energy for complexes between ligands and dimeric SARS-CoV2 M^{pro} (values kcal/mol).

Residue	$Lig1_{sub2}$	$Lig2_{Sub1}$	$Lig2_{Sub2}$	$Lig3_{Sub1}$	$Lig4_{Sub1}$	$Lig4_{Sub2}$	$Lig5_{Sub1}$	$Lig5_{Sub2}$	$Lig6_{Sub1}$	$Lig6_{Sub2}$	$Lig7_{Sub1}$	$Lig7_{Sub2}$
T25									−0.891			
L27	−0.185	−0.529	−0.447	−0.591		−0.684	−0.663		−0.675		−0.662	−0.568
H41	−2.507	−0.544	−0.611	−1.752	−0.672	−0.611	−1.079	−0.486	−2.520	−0.838		
C44									−1.719			
T45	−0.586								−3.105			
S46	−0.578								−1.761			
M49	−1.110			−2.972			−1.486	−0.874	−1.452	−1.543	−0.860	
L50				−1.449								
F140	−0.610		−0.992		−0.871	−1.352					−1.256	−1.284
L141	−0.961				−1.546	−2.391					−1.987	−1.465
N142	−1.456	−1.911	−1.567	−1.208	−0.642	−0.714		−0.854		−2.523	−0.962	−0.777
G143		−1.335	−1.460	−0.849		−1.369				−1.462	−0.841	−1.191
S144	−0.502	−0.717	−0.648		−0.859	−1.844				−0.132	−1.269	−1.106
C145		−1.592	−1.855	−1.125	−1.876	−2.287	−0.746	−0.596	−0.637		−1.960	−2.133
H163	−0.466	−0.925	−2.322		−1.626	−1.403	−0.709	−0.191			−1.465	−1.622
H164				−1.565	−1.065							
M165	−1.069		−0.748	−0.776	−1.732		−1.258	−2.432	−0.554	−2.578		−1.654
D166			−2.040		−3.466	−0.604					−2.836	−4.313
L167										−0.572		
R188										−1.492		
Q189							−1.521	−1.129		−2.417		

Indomethacin = lig1, naftazone = lig2, ofloxacin = lig3, zopiclone = lig4, sofosbuvir = lig5, pitavastatin = lig6, eszopiclone = lig7. Sub1 and Sub2 denote subunits 1 or 2 of dimeric SARS-CoV2 M^{pro}.

was not coupled to conformational changes of monomeric SARS-CoV2 M^{pro}. The binding of naftazone, pitavastatin, eszopiclone, perampanel, azelastine, celecoxib, ondansetron and lemborexant was linked to a decrease in the conformational mobility of monomeric SARS-CoV2 M^{pro}, and the conformational reduction would be coupled to an increase in the ΔG_{bind} value (Table 1), due to an unfavorable entropy component. The binding of zopiclone was coupled to an increase in the conformational mobility, which contributed to a decrease in the ΔG_{bind} value due to a favorable entropy component. The binding of lopinavir and ritonavir was linked to a decrease in the conformational mobility of monomeric SARS-CoV M^{pro}, which would also be linked to an increase in the ΔG_{bind} value observed in Table 1.

Analysis of the covariance values for free and bound dimeric SARS-CoV2 M^{pro} and SARS-CoV M^{pro} systems indicates that the binding of naftazone, zopiclone, sofosbuvir, eszopiclone, perampanel, azelastine, nelfinavir, praziquantel, lemborexant and lopinavir was not linked to important conformational changes of dimeric SARS-CoV2 M^{pro}, which means that their coupling with receptors would not impact the affinity observed in Table 2. The binding of ofloxacin, pitavastatin and fenoterol contributed to a decrease in conformational mobility, and the coupling of

Table 5
Per-residue free energy for complexes between ligands and dimeric SARS-CoV2 M^{pro} (values kcal/mol).

Residue	$Lig8_{sub1}$	$Lig8_{Sub2}$	$Lig9_{Sub1}$	$Lig9_{Sub2}$	$Lig10_{Sub1}$	$Lig10_{Sub2}$	$Lig11_{Sub1}$	$Lig11_{Sub2}$	$Lig12_{Sub1}$	$Lig12_{Sub2}$	$Lig13_{Sub1}$	$Lig13_{Sub2}$
T25			−1.271		−0.527							
L27	−0.776	−0.633	−0.737		−1.097	−0.572	−1.929		−0.141	−0.517	−0.831	−0.725
H41		−1.038	−0.528		−1.898	−1.611	−2.726		−0.556	−0.833	−1.449	−1.328
V42					−0.622							
T45			−0.544									
S46										−0.531		
M49	−1.669		−0.776		−2.057	−1.981			−1.216	−2.325	−1.516	
L50	−1.151									−0.761		
F140	−0.849	−0.918		−1.214							−0.627	−0.611
L141				−0.710							−0.526	−0.544
N142	−2.929	−2.445	−2.018	−1.194						−0.795	−0.735	−0.929
G143	−2.328	−2.454	−0.792				−0.650				−1.684	−1.672
S144	−1.672	−1.517				−1.247					−1.486	−1.415
C145	−1.566	−2.232	−1.109		−0.913		−1.598		−0.518		−3.112	−2.718
H163			−1.652	−0.707								
H164					−0.708		−0.560					
M165	−2.233	−1.841	−1.661	−3.722	−1.750	−1.667	−1.248	−3.034	−1.805		−1.984	−1.903
D166	−1.017		−0.950	−4.882				−0.849				
L167									−0.702			
P168									−0.778			
D187				−1.061			−1.119		−1.468			
R188				−0.659		−0.898		−1.323	−0.504	−0.969		
Q189				−1.367		−1.248		−2.608	−3.590	−1.936		−0.556
T190									−1.119			
A191									−2.158			
Q192				−0.988					−1.391			

Perampanel = lig8, fenosterol = lig9, azelastine = lig10, celecoxib = lig11, nelfinavir = lig12, praziquantel = lig13. Sub1 and Sub2 denote subunits 1 or 2 of dimeric SARS-CoV2 M^{pro}.

Table 6
Per-residue free energy for complexes between ligands and dimeric SARS-CoV2 M^{pro} and SARS-CoV M^{pro} (values kcal/mol).

Residue	$Lig14_{sub1}$	$Lig14_{Sub2}$	$Lig15_{Sub2}$	$Lig16_{Sub1}$	$Lig16_{Sub2}$	$Lig17_{Sub1}$	$Lig17_{Sub2}$	$*Lig16_{Sub1}$	$*Lig16_{Sub2}$	$*Lig17_{Sub1}$
T25								−0.614		
T26										
L27					−0.662			−0.741		
H41	−0.613		−2.124	−0.890	−1.138			−1.425	−0.757	−0.723
C44									−0.985	
S/A*46				−0.639	−0.699			−0.821	−0.604	
D48									−0.848	
M49			−2.513	−2.100	−2.211	−1.038	−2.367	−1.900	−2.314	−1.748
L50							−0.513		−0.875	−0.554
P52									−0.998	
L141	−0.859	−0.750								
N142	−0.654									
G143								−0.710		
C145	−0.598	−0.561					−0.663			
H163		−2.762								
M165	−1.787	−2.814	−0.647	−2.208	−3.300	−1.912	−1.979	−0.840	−1.234	−3.112
D166		−0.703								−1.830
L167				−0.700	−0.525	−0.850				−1.533
P168					−1.495	−2.062			−0.610	−1.946
H172		−0.549								
D187					−1.562	−0.778	−0.885			−0.764
R188							−0.843	−0.599	−0.972	
Q189		−0.709	−0.968		−1.951	−1.809	−0.785	−1.353	−1.069	−1.712
T190					−1.138	−0.782				
A191						−1.398				−0.543
Q192										−0.514

Ondansetron = lig14, lemborexant = lig15, lopinavir = lig16, and ritonavir = lig17. *denotes complexes between dimeric SARS-CoV M^{pro} with lopinavir (lig16*) and ritonavir (lig17*). Sub1 and Sub2 denote subunit 1 or 2 of dimeric SARS-CoV2 M^{pro} or SARS-CoV M^{pro}.

indomethacin, celecoxib, ondansetron and ritonavir was linked to an increase in dimeric SARS-CoV2 M^{pro}. However, the binding of lopinavir and ritonavir on dimeric SARS-CoV M^{pro} was not linked to conformational changes for lopinavir and an increase in the mobility of this receptor, which also means that their coupling on dimeric SARS-CoV M^{pro} did not impact the affinity observed in Table 2. Overall, this analysis shows that the binding of the best compounds on monomeric SARS-CoV2 M^{pro} or SARS-CoV M^{pro} more importantly impacts the ΔG_{bind} value estimated for each ligand due to the conformational changes coupled to the binding, whereas the affinity trends observed for the best compounds on the dimeric systems were not affected.

Table 7
Trace of the diagonalized covariance matrix of the backbone atoms for free and bound dimeric SARS-CoV2 and SARS-CoV M^{pro} systems.

System	Covariance (nm^2)
Dimeric SARS-CoV2 M^{pro}	
$SARS\text{-}CoV2_{apo}$	16.2
$SARS\text{-}CoV2_{indomethacin}$	20.8
$SARS\text{-}CoV2_{naftazone}$	15.0
$SARS\text{-}CoV2_{ofloxacin}$	12.0
$SARS\text{-}CoV2_{zopiclone}$	16.0
$SARS\text{-}CoV2_{sofosbuvir}$	16.3
$SARS\text{-}CoV2_{pitavastatin}$	13.2
$SARS\text{-}CoV2_{eszopiclone}$	15.3
$SARS\text{-}CoV2_{perampanel}$	17.4
$SARS\text{-}CoV2_{fenoterol}$	13.5
$SARS\text{-}CoV2_{azelastine}$	16.0
$SARS\text{-}CoV2_{celecoxib}$	18.4
$SARS\text{-}CoV2_{nelfinavir}$	15.9
$SARS\text{-}CoV2_{praziquantel}$	14.9
$SARS\text{-}CoV2_{ondansetron}$	20.9
$SARS\text{-}CoV2_{lemborexant}$	16.2
$SARS\text{-}CoV2_{lopinavir}$	15.2
$SARS\text{-}CoV2_{ritonavir}$	23.4
Dimeric SARS-CoV M^{pro}	
$SARS\text{-}CoV_{apo}$	21.0
$SARS\text{-}CoV_{lopinavir}$	20.9
$SARS\text{-}CoV_{ritonavir}$	25.1

4. Conclusion

In this research, we first performed the docking of 15 FDA-approved drugs, which were previously identified as potential inhibitors of monomeric SARS-CoV2 M^{pro}, by employing the recently elucidated crystallographic structure of monomer and dimeric SARS-CoV2 M^{pro}; then, 100-ns-long MD simulations coupled to the MM/GBSA approach were performed to compare results using both monomeric versus dimeric states, where the latter corresponds to the functional state. Additionally, similar studies were performed, including two known HIV-1 protease inhibitors, lopinavir and ritonavir, which have been previously employed as an effective therapy against SARS-CoV M^{pro}, to compare the inhibitory differences. Our results identified perampanel (best compound), praziquantel (second best compound) and nelfinavir (third best compound) as potential inhibitors of dimeric SARS-CoV2 M^{pro}, and these ligands also showed similar inhibitory properties than those of lopinavir and better inhibitory properties than those of ritonavir. Furthermore, comparative analysis of the affinity of lopinavir and ritonavir on SARS-CoV2 M^{pro} and SARS-CoV M^{pro} revealed that both compounds showed a higher affinity to SARS-CoV2 M^{pro}. On the basis of per-residue free energy decomposition, we identified the hot-spot residues (H41, M49, N142, G143, S144, C145, M165, D187, Q189, T190, A191 and Q192) which contribute significantly high to the total binding affinity. Among these residues H41 and C145 are conserved residues. Therefore, these key residues are important for drug binding. This study demonstrates for the first time that the coupling of ligands on dimeric SARS-CoV2 M^{pro} is linked to differences in the binding affinity in both subunits that may be characteristic of cooperativity. Our study also demonstrates that to obtain more confident drug discovery results, it is better to employ the dimeric state than the monomeric state since ligand binding on the monomer is coupled to conformational changes that contribute to the impact of the ΔG_{bind} value.

Declaration of competing interest

The authors declare that they have no known competing financial interests or personal relationships that could have appeared to influence the work reported in this paper.

Acknowledgements

The work was supported by grants from CONACYT (CB-A1-S-21278) and SIP/IPN (20201015).

Appendix A. Supplementary data

Supplementary data to this article can be found online at https://doi.org/10.1016/j.jmgm.2020.107762.

References

[1] N. Zhu, D. Zhang, W. Wang, X. Li, B. Yang, J. Song, X. Zhao, B. Huang, W. Shi, R. Lu, P. Niu, F. Zhan, X. Ma, D. Wang, W. Xu, G. Wu, G.F. Gao, W. Tan, N. Engl. J. Med. 382 (8) (2020) 727–733.
[2] H. Lu, C.W. Stratton, Y.W. Tang, J. Med. Virol. 92 (4) (2020) 401–402.
[3] B. Vastag, J. Am. Med. Assoc. 290 (2003) 1695–1696.
[4] V. Nukoolkarn, V.S. Lee, M. Malaisree, O. Aruksakulwong, S. Hannongbua, J. Theor. Biol. 254 (4) (2008) 861–867.
[5] Z. Xu, C. Peng, Y. Shi, Z. Zhu, K. Mu, X. Wang, W. Zhu, bioRxiv (2020), https://doi.org/10.1101/2020.01.27.921627.
[6] H. Yang, W. Xie, X. Xue, K. Yang, J. Ma, W. Liang, R. Hilgenfeld, PLoS Biol. 3 (10) (2005) e324.
[7] X. Xue, H. Yu, H. Yang, F. Xue, Z. Wu, W. Shen, X.C. Zhang, J. Virol. 82 (5) (2008) 2515–2527.
[8] Z. Ren, et al., The newly emerged SARS-like coronavirus HCoV-EMC also has an "Achilles' heel": current effective inhibitor targeting a 3C-like protease, Protein Cell 4 (2013) 248–250.
[9] Z. Ren, L. Yan, N. Zhang, Y. Guo, C. Yang, Z. Lou, Z. Rao, Protein & cell 4 (4) (2013) 248.
[10] F. Wang, C. Chen, W. Tan, K. Yang, H. Yang, Sci. Rep. 6 (2016) 22677.
[11] Z. Jin, X. Du, Y. Xu, Y. Deng, M. Liu, Y. Zhao, Y. Duan, Structure of M pro from SARS-CoV-2 and discovery of its inhibitors, Nature (2020) 1–5.
[12] B. Turk, Nat. Rev. Drug Discov. 5 (9) (2006) 785–799.
[13] P. Sang, S.H. Tian, Z.H. Meng, L.Q. Yang, RSC Adv. 10 (27) (2000) 15775–15783.
[14] V. Graziano, W.J. McGrath, L. Yang, W.F. Mangel, Biochemistry 45 (49) (2006) 14632–14641.
[15] D.S. Wishart, Y.D. Feunang, A.C. Guo, E.J. Lo, A. Marcu, J.R. Grant, T. Sajed, D. Johnson, C. Li, Z. Sayeeda, N. Assempour, I. Iynkkaran, Y. Liu, A. Maciejewski, N. Gale, A. Wilson, L. Chin, R. Cummings, D. Le, A. Pon, C. Knox, M. Wilson, Nucleic Acids Res. 46 (2018) D1074–D1082.
[16] M. J. Frisch, G. W. Trucks, H. B. Schlegel, G. E. Scuseria, M. A. Robb, J. R. Cheeseman, H. Nakatsuji, Gaussian 09, Revision D. 01. 2009, (Wallingford CT).
[17] G.M. Morris, R. Huey, W. Lindstrom, M.F. Sanner, R.K. Belew, D.S. Goodsell, A.J. Olson, J. Comput. Chem. 30 (2009) 2785e2791.
[18] D.A. Case, T.E. Cheatham, T. Darden, H. Gohlke, R. Luo, K.M. Merz Jr., R.J. Woods, J. Comput. Chem. 26 (2005) 1668e1688.
[19] Y. Duan, C. Wu, S. Chowdhury, M.C. Lee, G. Xiong, W. Zhang, P. Kollman, J. Comput. Chem. 24 (2003) 1999e2012.
[20] J. Wang, R.M. Wolf, J.W. Caldwell, P.A. Kollman, D.A. Case, J. Comput. Chem. 25 (2004), 1157e1174.
[21] W.L. Jorgensen, J. Chandrasekhar, J.D. Madura, R.W. Impey, M.L. Klein, J. Chem. Phys. 79 (1983), 926e935.
[22] T. Darden, D. York, L. Pedersen, J. Chem. Phys. 98 (1993), 10089e10092.
[23] W.F. Van Gunsteren, H.J.C. Berendsen, Mol. Phys. 34 (1977) 1311e1327.
[24] H.J.C. Berendsen, J.P.M. Postma, W.F. van Gunsteren, A. DiNola, J.R. Haak, J. Chem. Phys. 81 (1984), 3684e3690.
[25] W.L. DeLano, The PyMOL Molecular Graphics System, DeLano-Scientific, Palo Alto, CA, 2002.
[26] B.R. Miller, T.D. McGee, J.M. Swails, N. Homeyer, H. Gohlke, A.E. Roitberg, J. Chem. Theor. Comput. 8 (2012) 3314e3321.
[27] H. Gohlke, D.A. Case, J. Comput. Chem. 25 (2004) 238.
[28] A. Onufriev, D. Bashford, D.A. Case, Proteins 55 (2004) 383.
[29] M. Bello, J.E. Mendieta-Wejebe, J. Correa-Basurto, Biochem. Pharmacol. 90 (2) (2014) 145–158.
[30] S. Jeon, M. Ko, J. Lee, I. Choi, S.Y. Byun, S. Park, D. Shum, S. Kim, Antimicrob. Agents Chemother. 23 (7) (2020) 64, e00819-20.
[31] S. Yang, S.J. Chen, M.F. Hsu, J.D. Wu, C.T.K. Tseng, Y.F. Liu, W.C. Chen, J. Med. Chem. 49 (16) (2006) 4971–4980.
[32] C.Y. Wu, J. T Jan, S.H. Ma, C.J. Kuo, H.F. Juan, Y.S.E. Cheng, F.S. Liang, Proc. Natl. Acad. Sci. Unit. States Am. 101 (27) (2004) 10012–10017.
[33] C. Huang, P. Wei, K. Fan, Y. Liu, L. Lai, Biochemistry 43 (2004) 4568–4574.